Journal of Nondestructive Evaluation, Vol. 16, No. 4, 1997

A Novel Multi-Probe Resistivity Approach to Inspect Green-State Metal Powder Compacts

J. Stander,[1] J. Plunkett,[1] W. Michalson,[1] J. McNeill,[1] and R. Ludwig[1]

Received February 2, 1997; September 6, 1997

This paper describes a new instrumentation approach to the nondestructive testing of green-state powdered metallurgy components. These samples are likely to generate surface-breaking and subsurface defects prior to sintering. Exploiting the principles of electric resistivity or potential drop measurements in solids, a system is configured which is capable of recording surface voltage distributions due to impressed current inputs. At the heart of this novel testing procedure is a multiple-pin sensor which allows for flexible measurement conditions in order to cover wide surface areas. Practical tests with production samples compare well with both analytical and numerical modeling techniques in predicting surface voltage distributions. Furthermore, initial studies of surface-breaking flaws exhibit excellent defect detectability.

KEY WORDS: Green-state powder metallurgy compacts; resistivity testing; multi-probe sensor.

1. INTRODUCTION

The nondestructive testing of finished, postsintered powdered metallurgy (P/M) parts has primarily relied on traditional NDE techniques such as ultrasonic and eddy current inspections.[1] From a manufacturing point of view, it is however very desirable to detect the occurrence of cracks in the compacting stage prior to sintering. At this point, the PM compounds or green parts have been subjected to mechanical compression where press alignment, tooling, and material mixtures play a major role in determining the quality of the final part.[2] An NDE technique at this stage would permit the interception and modification of the manufacturing process before sintering, thus avoiding the production of often thousands of faulty end specimens at associated high costs. Unfortunately very little work has been devoted toward the inspection of green parts,[3] since the loosely-connected microscopic particle compositions represent high attenuation to elastic waves. In addition, electromagnetic properties, primarily the low conductivity, the often ferrous material nature as well as high surface reflectivity to heat energy make PM parts not suitable for eddy current and thermal inspections.

The focus of this investigation is concentrating on the electric resistivity or impedance properties of P/M parts,[4–7] mainly because

- they possess sufficient conductivity/resistivity which can be exploited as a physical quality parameter,
- the testing methods appear sufficiently robust in that small production-related changes in material composition such as density variations do not impede the detection of cracks, and
- the equipment development is not prohibitively expensive.

It is pointed out that this type of testing exploits spatial changes in conductivity only, i.e., the mechanical processes of compacting and machining must be correlated with a single electric material parameter.[8] The associated mathematical task of inverting the underlying

[1] Department of Electrical and Computer Engineering, Worcester Polytechnic Institute, Worcester, Massachusetts 01609.

0195-9298/97/1200-0205$12.50/0

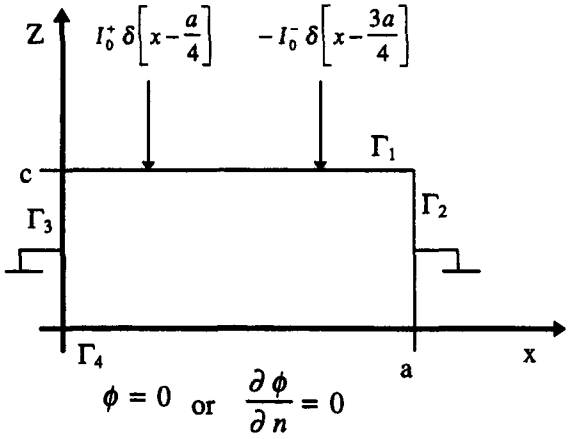

Fig. 1. Generic test configuration of a cross-section of a rectangular PM part with point currents located at surface.

elliptic partial differential equations for the unknown conductivity distribution has yielded rather low quality images as the medical field has shown.[9]

From an instrumentation point of view, sensitivity and reproducibility have to be established. Key points of the investigation include such parameters as flaw size and orientation vs. detectable voltage response, number and placement of sensors, contact needle pressure, current strength, conductivity variations from sample-to-sample as well as within the individual sample, etc.

In order to aid in the preparation of controlled samples as well as providing data for the instrumentation effort, a theoretical model attempting to simulate physical reality is necessary. On the basis of the finite element method, a numerical model has been devised which predicts voltage distributions due to current source inputs. Results from this model are subsequently employed to calibrate the voltage recording of the instrument.

The organization of this paper is as follows: Sect. 2 introduces the basic theory and the generic model configuration followed by the numerical formulation and its analytical verification. Section 3 then discusses the analog and digital instrumentation approach which allows the recording of surface voltage distributions based on known current inputs. In Section 4, preliminary measurement results of P/M specimens are placed in context with the theoretical modeling approach.

2. THEORETICAL BASIS

The DC impedance testing of green-state P/M parts can mathematically be described as a static current flow problem. Current input and current output to the specimen are modeled by imposing Neumann-type of boundary conditions at point locations on the surface. The injected current establishes electric field and potential distributions throughout the sample region as well as over the surface. It is the differential voltage between point contacts on the surface which is of interest since it is measured by our instrument. Therefore the starting point of the theoretical analysis is Laplace's equation in the form

$$\nabla \cdot [\sigma \nabla \phi (\mathbf{r})] = 0 \tag{1}$$

where $\phi(\mathbf{r})$ is the voltage distribution, and σ represents the spatially dependent conductivity. The localized source current density at discrete surface locations is applied through the boundary condition

$$\sigma \frac{\partial \phi}{\partial n} = -J \tag{2a}$$

while over the remaining surface locations either flux free, or potential

$$\phi = \phi_0 \tag{2b}$$

conditions are imposed. Since closed-form solutions to Eq. (1) can only be found for the simplest geometric cases, numerical methods such as finite difference, finite elements, boundary elements are employed when realistic problems have to be investigated. In particular, the finite element approach converts Eq. (1) into a linear matrix equation

$$[S]\{\phi\} = \{J\} \tag{3}$$

where $[S]$ contains spatial information regarding σ and vectors $\{\phi\}$ and $\{J\}$ denote the unknown nodal potential and known source distributions throughout the solution domain.[2] The nodal potential values $\{\phi\}$ can subsequently be processed into voltage distributions $\phi(x, z)$ via suitable local approximation or shape functions. With ϕ determined via matrix inversion, the electric field $\mathbf{E}$ is found through the gradient operation $\mathbf{E} = -\nabla\phi$. A basic electrostatic test configuration for an unflawed sample of length a is shown in Fig. 1. In this model one injects and receives a known current I_0 along Γ_1 which is specified as Neumann-type boundary condition. The location of the point current contacts at $a/4$ and $3a/4$ are described by shifted delta functions $\delta(x - a/4)$ and $\delta(x - 3a/4)$ of strength I_0^+ and I_0^-. In addition, the following boundary conditions are imposed:

$$\text{on } \Gamma_2 \text{ and } \Gamma_3\text{: } \phi = 0 \tag{4a}$$

$$\text{on } \Gamma_4\text{: either } \phi = 0 \tag{4b}$$

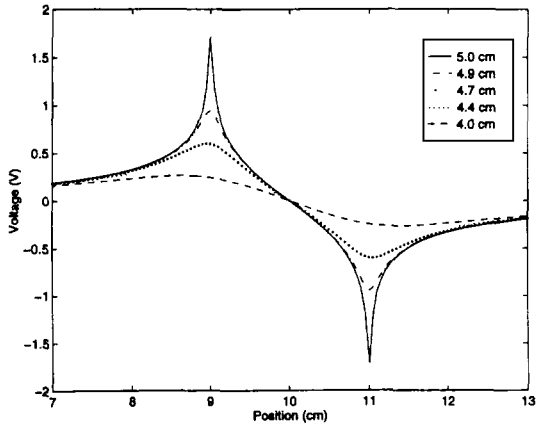

Fig. 2. Voltage distribution as a function of depth for $\phi(x, 0) = 0$.

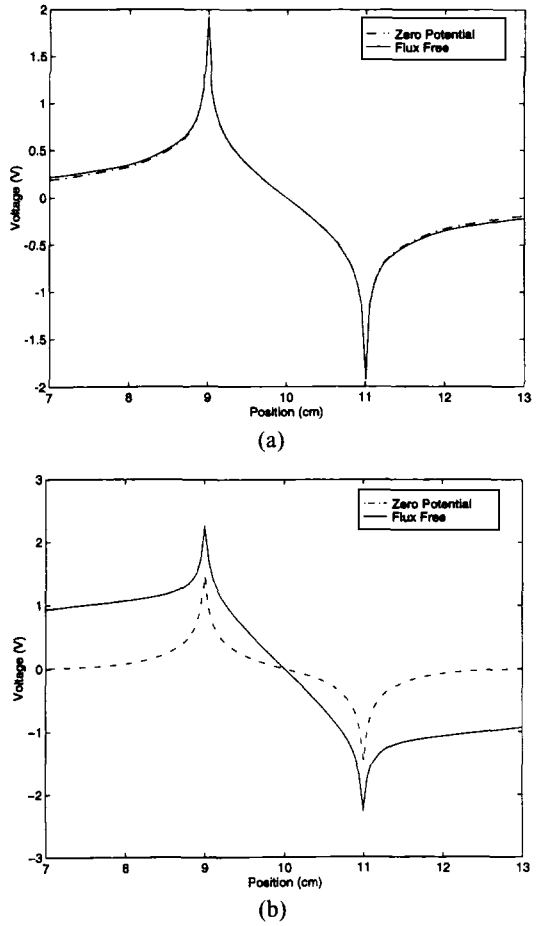

Fig. 3. Voltage distribution $\phi(x, c)$ for potential fixed ($\phi(x,0) = 0$) and flux free boundary conditions as a function of sample thickness for (a) c = 5 cm, and (b) c = 3 cm.

$$\text{or } \frac{\partial \phi}{\partial n} = 0 \tag{4c}$$

In order to test the fidelity of the numerical model for the geometry depicted in Fig. 1, analytical solutions are derived based on a standard Separation of Variable (SOV) approach which yields for boundary condition type (4b)

$$\phi(x, z) = \frac{2}{\pi} \sum_{n=1}^{\infty} \frac{1}{n \cosh(c\,\alpha_n)} \left[I_0^+ \sin(n\,\alpha_n\, a/4) + I_0^- \sin(n\,\alpha_n\, 3a/4) \right] \sin(\alpha_n x) \sinh(\alpha_n z) \tag{5}$$

and for boundary condition type (4c)

$$\phi(x, z) = \frac{2}{\pi} \sum_{n=1}^{\infty} \frac{1}{n \sinh(c\,\alpha_n)} \left[I_0^+ \sin(n\,\alpha_n\, a/4) + I_0^- \sin(n\,\alpha_n\, 3a/4) \right] \sin(\alpha_n x) \cosh(\alpha_n z) \tag{6}$$

where $\alpha_n = \frac{n\pi}{a}$ and I_0^+, I_0^- are the impressed positive and negative currents. Both boundary conditions can easily be enforced in the experiment by either grounding the bottom surface or by placing the PM sample on an insulating contact plane. For instance, with current of +/− 1 A, a = 20 cm, c = 5 cm, Fig. 2 shows five typical voltage distributions at various depth layers starting from the top surface (z = 5 cm) down to z = 4 cm. Figure 3 quantifies the effect of sample thickness variations for the two types of boundary conditions imposed on Γ_4. As expected, both solutions (5) and (6) yield the same surface voltages for a thick sample (Fig. 3a), but begin to differ as the sample thickness is reduced (Fig. 3b). The drop in maximum voltage signal strength as a function of depth into the specimen is depicted in Fig. 4 for grounded Γ_4. Here z = 5 cm corresponds again to the surface location at the positive current injection point x = $a/4$ = 5 cm. To appreciate the fidelity of the finite element method, Fig. 5 compares the numerical predictions with the flux-free voltage distribution of a 5-cm-thick sample.

To extend the numerical model to simulate a surface-breaking flaw of 0.5 mm width and 3 mm depth, Fig. 6 shows the surface voltage distribution across the flaw versus the no-flaw situation. Since the flaw is mod-

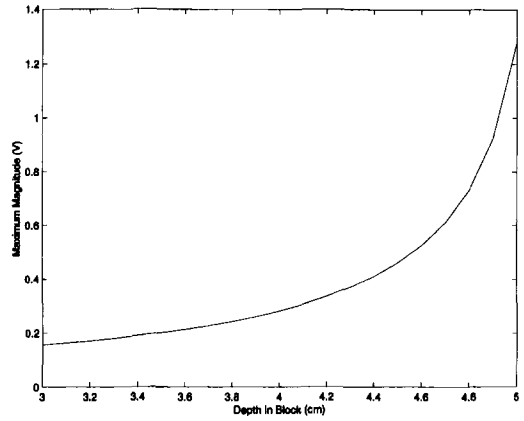

Fig. 4. Maximum signal strength as a function of sample depth.

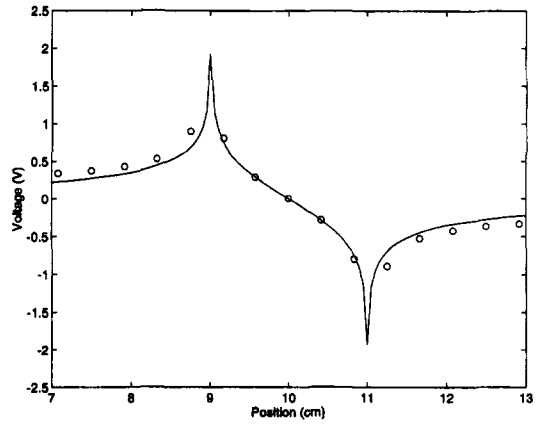

Fig. 5. Comparison between analytical solution (solid line) and numerical prediction (circles) for flux-free boundary condition.

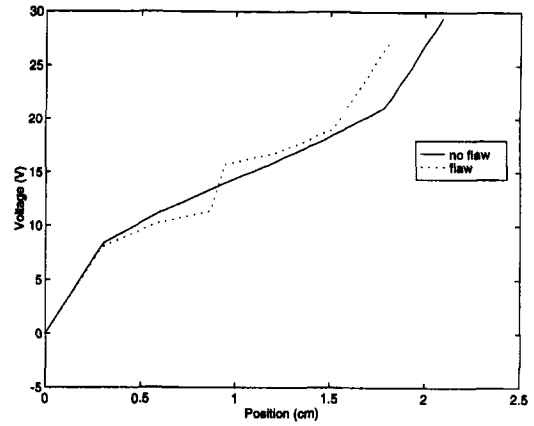

Fig. 6. Numerical surface voltage prediction for no-flaw and surface-breaking flaw condition.

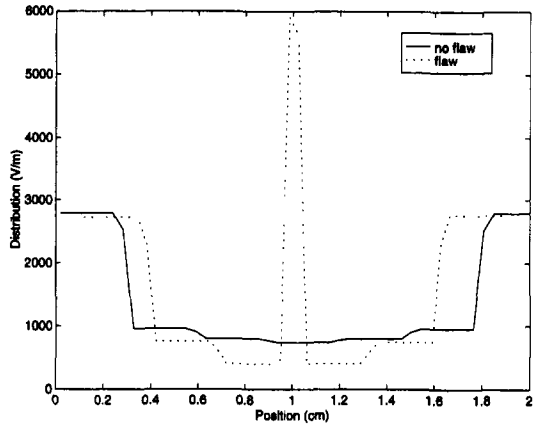

Fig. 7. Surface gradient predictions of Fig. 6.

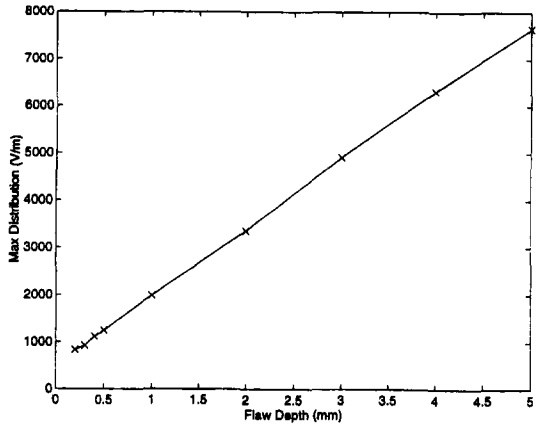

Fig. 8. Flaw depth as a function of recorded surface voltage gradient.

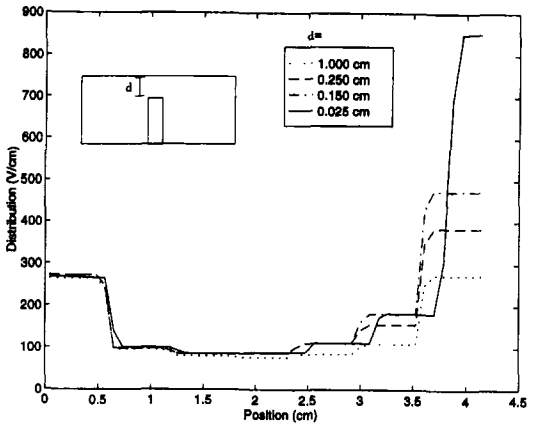

Fig. 9. Cross-sectional 2-D simulation of a growing subsurface defect. The flaw is initially 1 cm below the surface and extends all the way to the bottom. The distance flaw tip-sample surface, d, is then reduced to 0.25 cm, 0.15 cm, and 0.025 cm.

eled as a discontinuity in conductivity from $\sigma_0 = 20$ *S/m* to $\sigma = 0$, one observes a localized increase in the surface voltage slope. As expected, in moving beyond the flaw region the voltage approaches again the no-flaw distribution.

The increase in the surface voltage gradient across the flaw suggests a differential voltage plot as shown in Fig. 7 which clearly delineates the flaw location and its depth profile. In fact, plotting flaw depth as a function of peak value of the recorded surface voltage gradient results in a linear graph as shown in Fig. 8. An increasing subsurface flaw is simulated in Fig. 9 where a 0.5-mm-wide and 2-cm-long inclusion is growing toward the surface in five increments.

3. ANALOG AND DIGITAL INSTRUMENTATION

In order to exploit the physical principles of the impedance measurement technique an instrument has been constructed which is capable of injecting a constant current into the P/M compact and which samples the resulting voltage distribution on the surface accurately and repeatably. A key feature of this instrument is a multiprobe sensor depicted in Fig. 10. The sensor consists of spring-loaded (sharp tip) pins configured in a planar square array. The outer probes are used to inject current and the inner probes record the voltage distri-

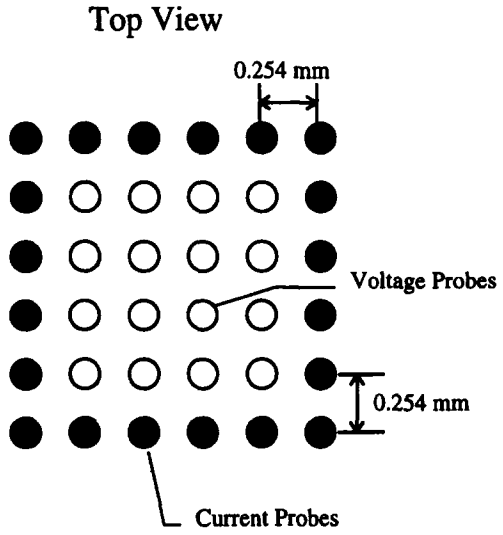

Fig. 10. Multiprobe sensor consisting of an array of 8 × 8 spring-loaded needles.

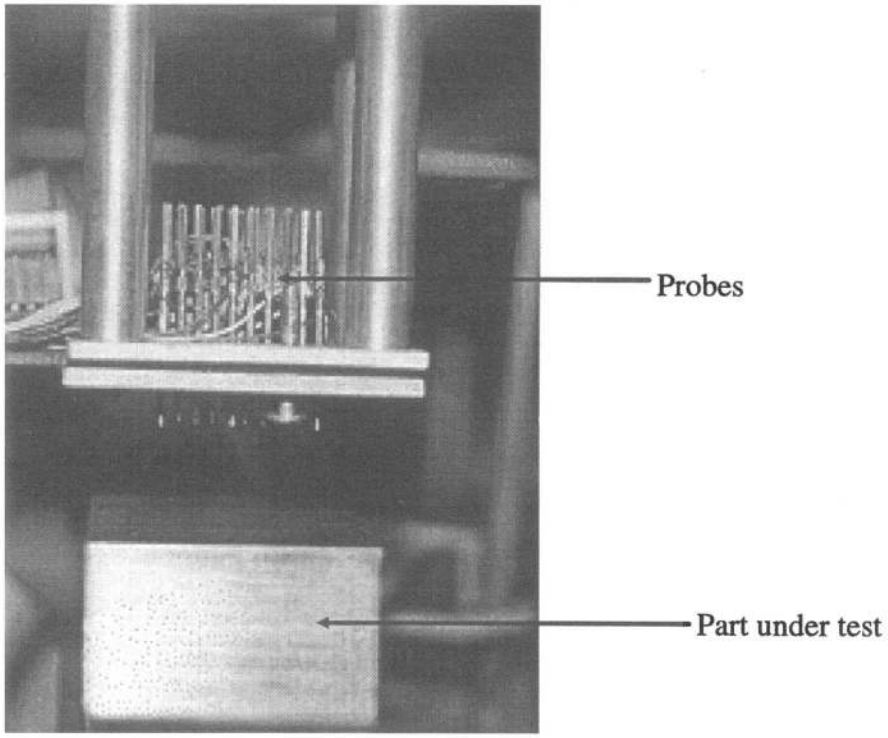

Fig. 11. Sensor in contact with green-state P/M part.

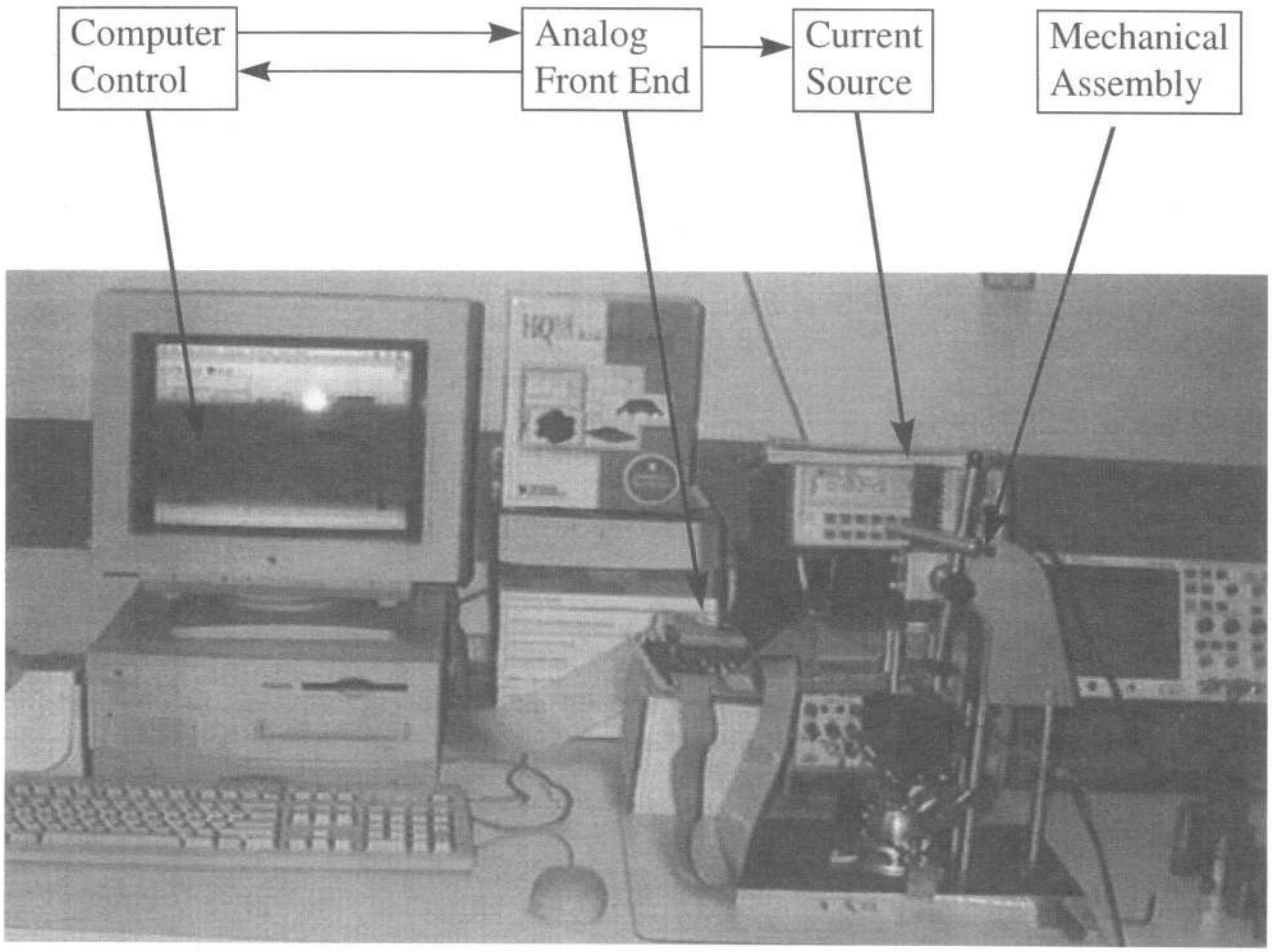

Fig. 12. Block diagram of instrument.

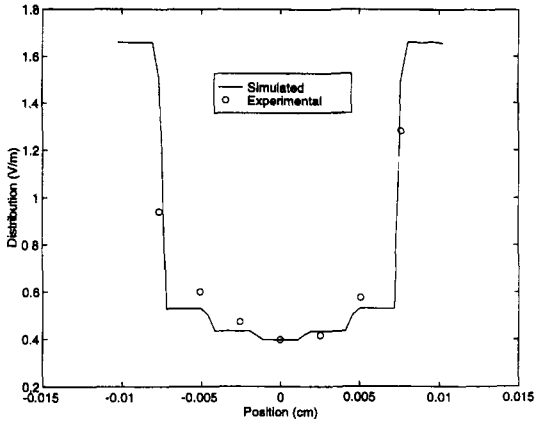

Fig. 13. Computed and measured voltage gradient over the surface of an unflawed P/M part.

bution. Since we rely on differential voltage processing (see Fig. 7), the system has to record signals between nearest neighbor pins. This configuration yields high flexibility and large surface coverage of the P/M part. To maximize the flaw signal response, the voltage is initially recorded at an orthogonal direction with respect to the current flow. At present the measurement array consists of an 8 × 8 pin array with a pin-to-pin spacing of 2.54 mm resulting in a 37.6 mm^2 planar sensor area which contacts the P/M part having a total surface area of 50 mm × 75 mm (Fig. 11). The spacing is chosen to ensure maximum surface coverage while maintaining sufficient measurement accuracy.

To acquire and process these voltages several system components are required as shown in Fig. 12. A

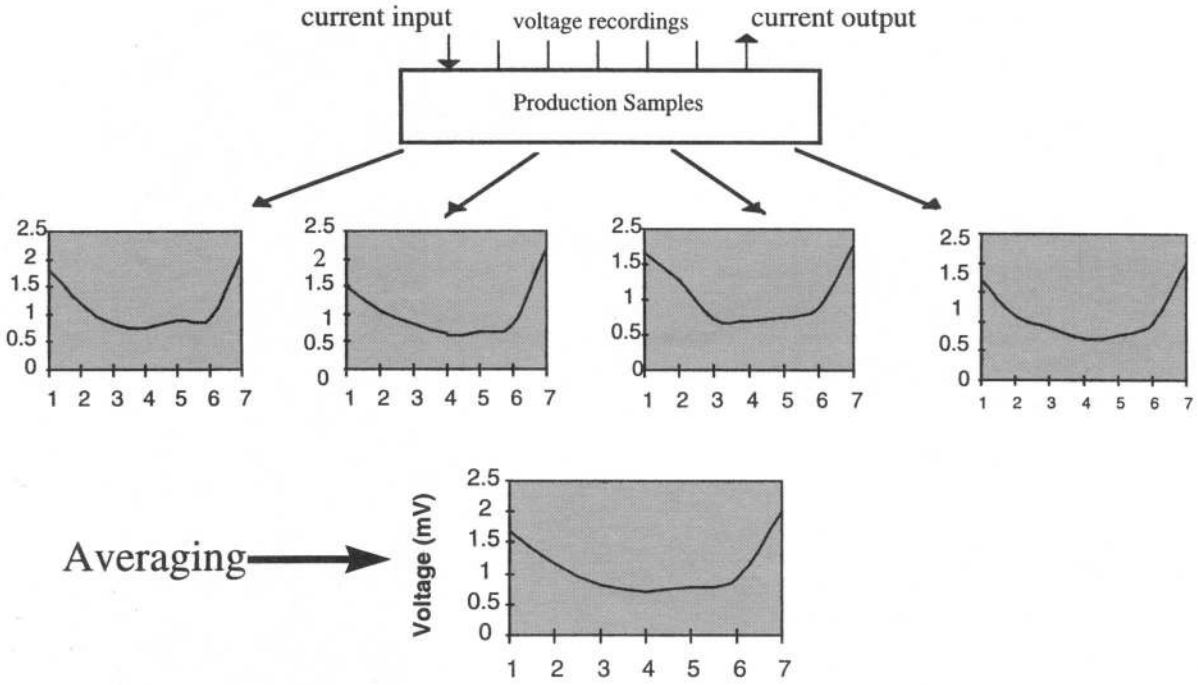

Fig. 14. Voltage averaging over four production green-state P/M samples in order to establish a baseline.

constant current source injects a DC current of up to 1A into the outer pins of the probe. Through a mold the P/M part is positioned accurately under the multipin sensor to ensure repeatable measurements from sample to sample. The probe is attached to an arbor press which mechanically brings the sensor in contact with the part for good electrical contact. Under computer control sensor pins can then be selected for current input as well as voltage recording. The selection of the various voltage pins is achieved with the aid of an analog multiplexer. Because the acquired voltages are on the order of a few mV, analog signal processing is required to amplify and filter the signals. A 12 bit analog-to-digital converter saves the data in files for further digital processing and display. The software control is handled through the LabView package of National Instruments.

4. MEASUREMENT RESULTS

The instrument was first used to record voltage measurements on unflawed samples to establish a baseline and to compare the practical data against the theoretical modeling predictions. Figure 13 provides measured and computed gradient voltages over the surface of a P/M part. Even though the agreement is in general good, one should keep in mind several possible error sources. First, the simulation model assumes an homogeneous sample whereas in reality parts have often statistically known variations in homogeneity. In addition, shape and size of the part can cause edge effects not taken into considerations by the theoretical model. Finally, errors associated with small misalignments of the probe placement can influence the voltage recording. Since these errors occur in a predictable manner, they can be taken into account by establishing a baseline as discussed below.

As a next step, the prototype was applied to the testing of surface breaking flaws in production samples. Since the surface voltage profile, even for unflawed samples, changes slightly from sample-to-sample due to contact misalignments and manufacturing-related variations in density and material composition, a baseline was established. This can be accomplished by averaging the measured voltage distribution over several specimens as shown in Fig. 14 for four unflawed samples. To obtain an appreciation of the type of surface-breaking flaw that can be detected, Fig. 15 depicts the magnified cross-section of a typical hair-line crack with a surface opening of approximately 100 microns and a depth of 1.6

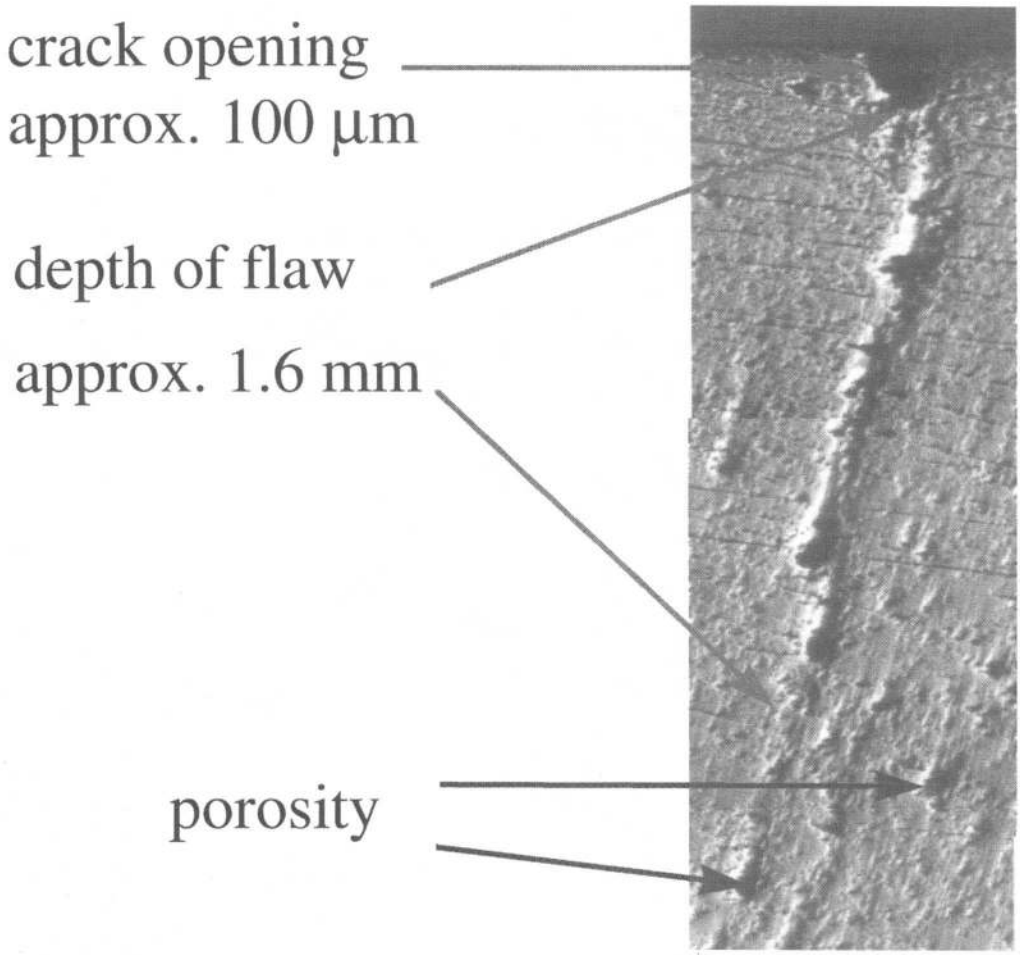

Fig. 15. Cross-section of a typical surface-breaking flaw.

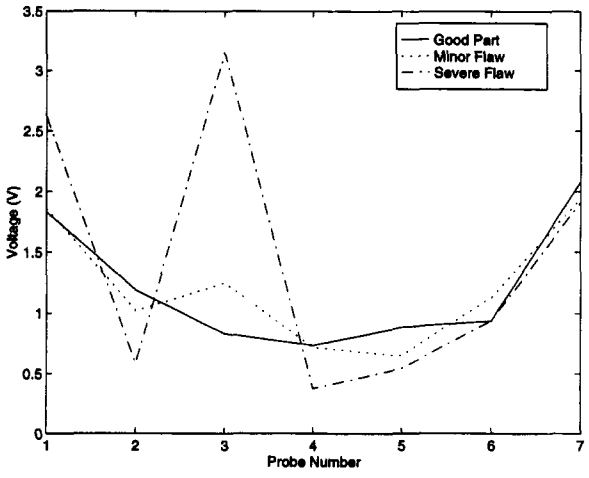

Fig. 16. Voltage distribution of three production green-state P/M samples.

mm. In Fig. 16, the response of a minor flaw vs. major flaw against the baseline response is presented for current injection and voltage recordings perpendicular to the surface flaw length. The severe flawed distribution demonstrates an increase of more than 4 times the voltage response compared to the baseline, while the less severe flaw still doubles in value. Figure 17a and b quantify the surface opening of (a) a severe flaw which ranges in size between 61 to 188 microns, and of (b) a minor flaw which ranges in size between 7 and 30 microns. In order to establish a baseline, voltage distributions are examined which represent no flaw, minor, and severe surface breaking flaws. The measurements taken by the experimental arrangement are very repeatable and with a typical 66 dB signal-to-noise (SNR) ratio provide an excellent resolution.

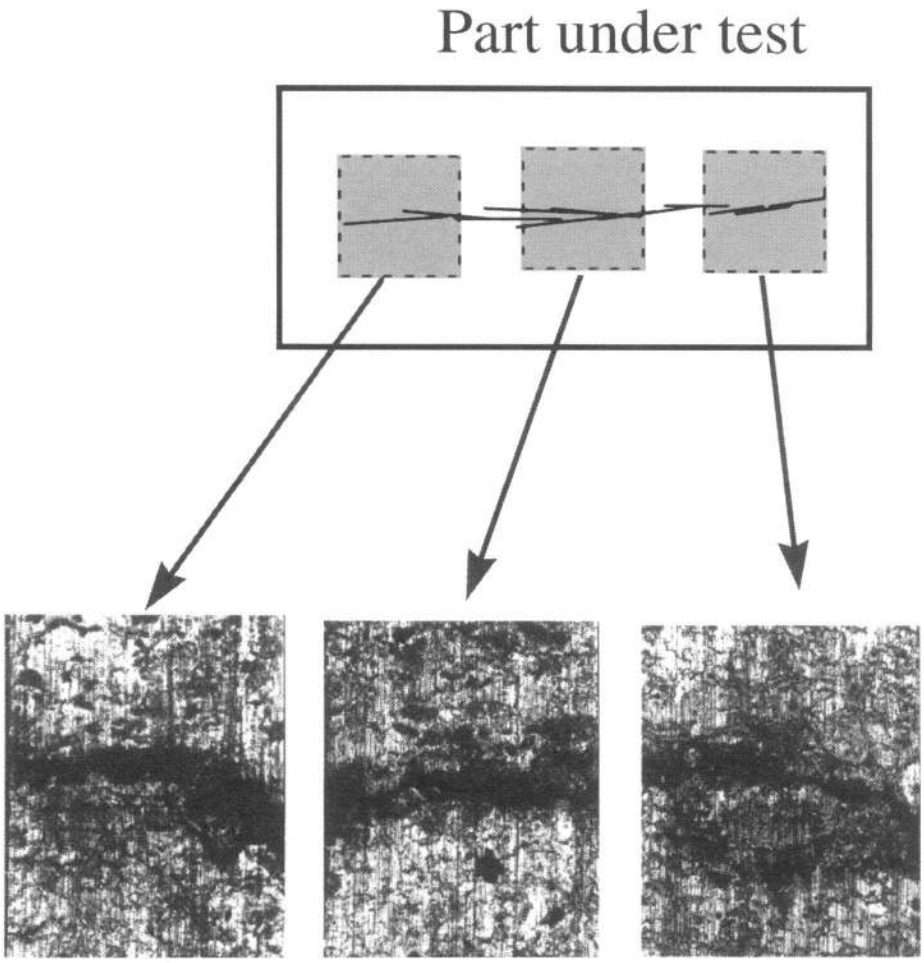

Fig. 17. Microscopic surface-openings of (a) a major surface-breaking defect.

5. CONCLUSIONS

In this paper, we have introduced electric resistivity testing as a successful approach to inspect green-state P/M compacts. By relying on both analytical and numerical modeling techniques it is shown that the physical behavior of current flow in solid media can be adequately described by a static flow phenomena. Furthermore, model predictions can be brought into agreement with practical measurements on production samples. Based on these physical principles an instrumentation approach has been devised which relies on a novel multiprobe sensor capable of injecting source currents and recording voltage responses over a single plane, wide sample surface area. It is demonstrated that surface breaking cracks on the order of 100 microns in green-state production samples can be detected. This bodes well for the inspection of more complex geometries as well as corner effects which requires nonplanar multisensor configurations that have to be custom-tailored to a particular sample.

Since the main emphasis of this paper has been the development of a new P/M inspection instrument, discussions of particular detection algorithms which relate the surface voltage recordings to the flaw geometry are deferred to an upcoming companion paper.

ACKNOWLEDGMENTS

The authors are grateful to Dr. D. Ostergaard of ANSYS, Inc. for his support of the numerical simulations in this paper. Dr. L. Pease of Powder Tech, Inc. was instrumental in providing technical expertise regarding the P/M sample preparations.

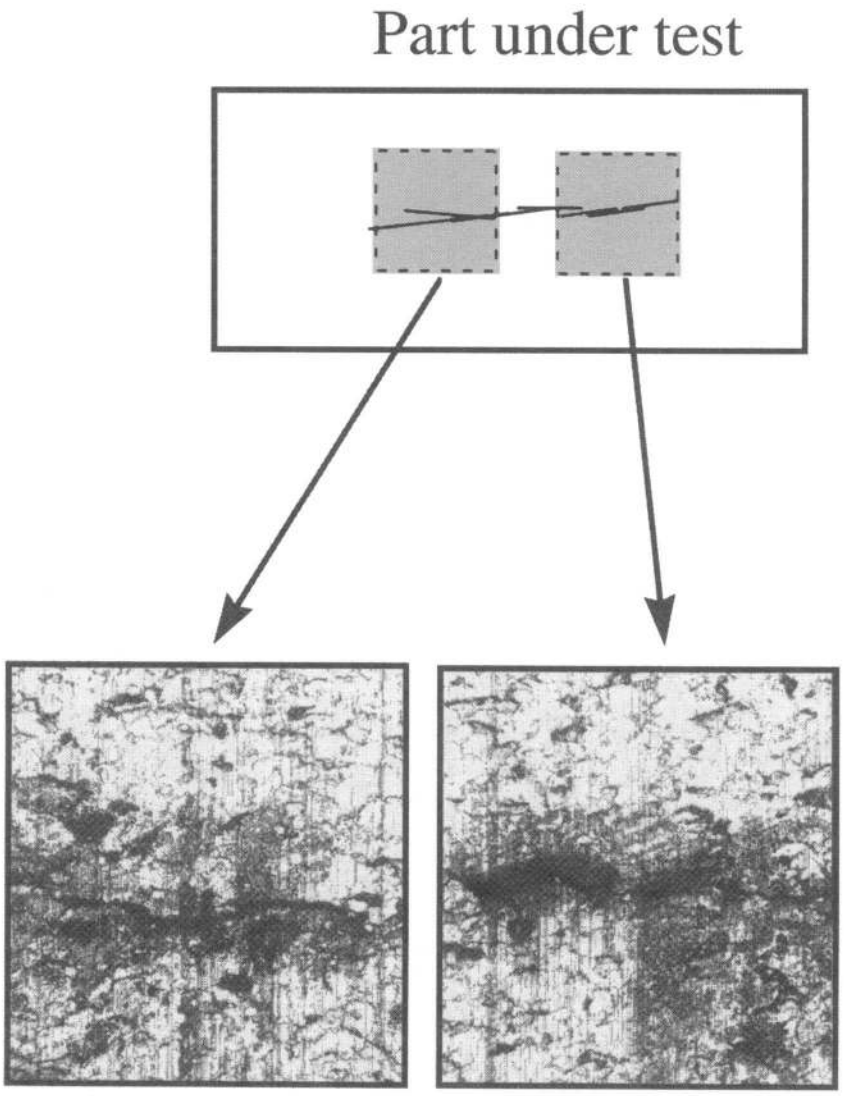

Fig. 17. Continued. Microscopic surface-openings of (b) minor surface breaking defect.

REFERENCES

1. L. F. Pease, Flaw Detection in P/M Parts via Real-Time X-Ray Analysis, Eddy currents and electrical resistivity. *International Powder Metallurgy Conference* (1988), pp. 478–480.
2. D. Zenger and H. Cai, The Common Cracks in Green P/M Compacts Handbook, Powder Metallurgy Research Center Report, Worcester Polytechnic Institute, Worcester, MA (March 1996).
3. L. F. Pease, Crack Detection in Green and Sintered P/M Parts. Presented at the *Powder Metallurgy World Congress*, San Francisco (June 21–26, 1992).
4. R. L. Cohen and K. W. West, Characterization of metals and alloys by electrical resistivity measurements, *Mater. Eval.* **41**:1074–1077 (1983).
5. S. Nath, T. J. Rudolphi, and W. Lord, Comparative study of finite element and boundary element analysis of the DC potential drop method. *Mater. Eval.* **50**:51–55 (1992).
6. A. Lewis and D. Bush, Resistivity measurements of evaluation of coating thickness. *Mater. Eval.* **49**:132–135 (1991).
7. H. M. Bauschke and K. H. Schwalbe, Measurement of the depth of surface cracks using the direct current potential drop method. *Zeitsch. Werkst.* **16**:156–165 (1985).
8. E. R. Leheup and J. R. Moon, Electrical conductivity changes during compaction of pure iron powder. *Powder Metall.* **4**:195–198 (1978).
9. H. M. Powell, D. C. Barber, and I. L. Freeston, Impedance imaging using linear electrode arrays. *Phys. Physiol. Meas.* **8**:109–118 (1987).
10. A. Uhlir, The potentials of infinite systems of sources and numerical solutions of problems in semiconductor engineering. *Bell Syst. Technol. J.* 105–128 (1995).
11. G. H. Aronson and R. O. Ritchie, Optimization of the electric potential technique for crack growth monitoring on compact test pieces using finite element analysis. *J. Test. Eval.* **7**:208–215 (1979).